2011, 15th Int. Conf. on Advanced Robotics (ICAR'11), Pages 112-117, Tallinn, Estonia 2011.
DOI : 10.1109/ICAR.2011.6088585

Reactive path planning for autonomous sailboat

Clément Pêtrès, Miguel-Angel Romero-Ramirez, Frédéric Plumet

***Abstract*— Among Autonomous Surface Vehicle (ASV), sailboat robots could be an efficient solution for long term missions and semi-persistent presence in the oceans since they rely on renewable energy like solar and wind energy. However, steering of such vehicles presents an inherent difficulty since the thrust force heavily rely on the wind (speed and direction) and sail angle as well as on the underlying complex dynamic properties, mainly due to the aero and hydrodynamic forces acting on the ship. This paper proposes a new reactive path planning method which takes into account the so called no-go zones and turns them into virtual obstacles. Then, a potential field algorithm is applied to drive the sailboat towards the goal while avoiding obstacles even when the goal is located directly downwind or upwind. Simulations, using a boat specific dynamic simulator, show that the proposed method can successfully drive an autonomous boat between a set of predefined way-points under time varying wind conditions. This method is computationally efficient and is suitable for on-board real-time implementation.**

I. Introduction

During the recent years, a growing activity concerning autonomous surface vehicles have been noted. Applications for such vehicles include port protection, mines countermeasure, reconnaissance and surveillance mission [1]–[3]. One of the probably most important reason that can explains this growing activity is the need for better understanding of the complex interactions between atmosphere and oceans as well as environmental monitoring. Global warming, meteorological and ecological studies in particular need better characterization of ocean processes and consequently requires a broad spectrum of observational tools to understand the complex dynamic coupling between the Earth's oceans and the atmosphere.

Ocean sensing have been typically done with satellites, airplanes, buoys, research vessels or ship of opportunity. However, satellites and airplanes are limited by cloud cover, temporal/geographical coverage, as well as spatial resolution. Manned research vessels are expensive to deploy and usually suffer from a weak of availability. Spatial sampling is impossible with moored buoys and they cannot be self-deployed to specific areas of interest. Over the last decades, the growing needs of the oceanographic community for in-situ measurements and complementary observing systems have stimulated the robotic community of academic researchers as well as private companies. Thus, considerable progress have been observed in the development and use of autonomous marine platform such as drifters, gliders, autonomous underwater vehicles (AUV), and autonomous surface vehicles (ASV). Each of these platforms provides various capabilities for payload, endurance, range, communication, mobility, and autonomy. In the recent years, numerous ASV have been developed for bathymetry data recording in shallow water [4], monitoring of various marine environmental data either alone [5]–[7] or as part of a sensor network [8]–[12]. All of these aforementioned vehicles are conventional electric powered systems and suffer from a lack of autonomy that restrains their usage to short term missions. Sailboat robots could be an efficient solution for long term missions and semi-persistent presence in the oceans since they rely on renewable energy like solar and wind energy [13], [14]. However, steering of such vehicles presents an inherent difficulty since the thrust force heavily rely on the wind (speed and direction) and sail angle as well as on the underlying complex dynamic properties, mainly due to the aero and hydrodynamic forces acting on the ship.

This paper proposes a routing strategy for the computation of a suitable boat heading to reach a given way-point. Since accurate weather forecasts are not available for short distances and periods, our algorithm takes into account only local and instantaneous wind conditions to compute an optimum heading for the vessel. The path planning algorithm will react to changes of the wind conditions as well as detected obstacles in real-time by recalculating the heading periodically, similarly to what a human sailor do on a short regatta. This method have been successfully tested in simulation under various wind conditions, using a numerical simulator specifically tuned for the sailboat prototype that will be used.

II. Sailboat modeling

In this section the dynamic model of our prototype is presented. Both aero and hydrodynamic forces acting on the sailboat are taken into account to derive a realistic and computationally efficient numerical simulator.

A. Aero and Hydrodynamic Forces

The energy of the wind is transmitted to the system through the sails. The force given by the sail can be expressed in terms of lift and drag components, both applied in a center of effort. The magnitudes of these forces are related to the lift coefficient C_l and the drag coefficient C_d and can be calculated, in a sail reference frame, by the formulas of fluid mechanics (1).

$$\begin{cases} F_D &= \frac{1}{2}\rho S V^2 C_d \\ F_L &= \frac{1}{2}\rho S V^2 C_l \end{cases} \quad (1)$$

This work is supported by the ANR project ASAROME (Num. ANR-07-ROBO-0009)

UPMC Univ Paris 06, ISIR (Institut des Systèmes Intelligents et de Robotique) CNRS - UMR 7222 4 place Jussieu, 75005 Paris - France firstname.lastname@isir.upmc.fr

2011, 15th Int. Conf. on Advanced Robotics (ICAR'11), Pages 112-117, Tallinn, Estonia 2011.
DOI : 10.1109/ICAR.2011.6088585

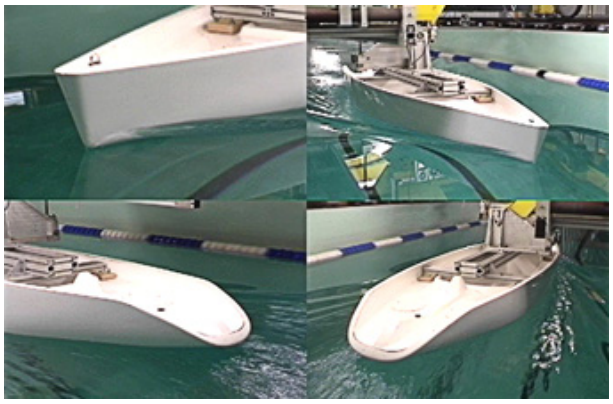

Fig. 1. Hull attached to a 6 components force-torque sensor in ECN towing tank

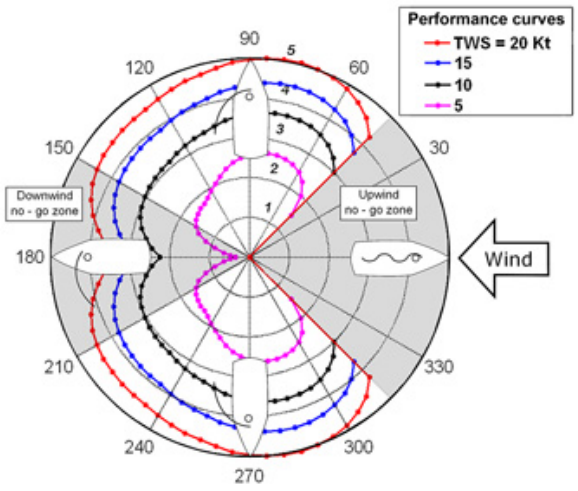

Fig. 2. Speed polar diagram of our sailboat

where ρ is the air density, S is the sail area and V is the apparent wind speed relative to the sail.

Since the rudder and keel are airfoil-shaped bodies moving through a fluid, the hydrodynamic forces acting on these elements can also be computed using an expression similar to (1) and replacing ρ by water density, V by the relative water velocity and by using the specific lift and drag coefficients for the rudder and keel.

The hydrodynamic forces acting on the hull can be written as (2) where $R_{Friction} + R_{Residuary}$ is the evaluated resistance without leeway (angle between the boat main axis and the velocity vector) and heel (roll angle), R_{Leeway} is the leeway induced resistance and R_{Heel} is the heel induced resistance [15].

$$R_{Hydro} = R_{Friction} + R_{Residuary} + R_{Leeway} + R_{Heel} \qquad (2)$$

Since the geometry of the hull is compliant with the Delft systematic series, $R_{Residuary}$ can be computed using the Gerritsma model with a scale factor based on Froude number [16], [17].

The other components $R_{Friction}$, R_{Leeway} and R_{Heel} of the total hull's hydrodynamic resistance are then experimentally identified using the towing tank ($150m \times 5m \times 3m$) of *Ecole Centrale de Nantes*. The hull, without keel and rudder, was mounted on a six DoF force-torque sensor with non restricted heave and sway (Fig. 1) and the resulting forces and torques have been recorded under various traction conditions (no-heel and no-leeway, heel angle and no-leeway, leeway angle and no-heel, leeway and heel angle) and for a broad range of ship velocity.

Based on the data recorded during the tests, a set of interpolated functions has been derived to model each component of the total hydrodynamic resistance.

B. Motion Equation and Simulator

The sailboat motion equations can be written using the Newton-Euler's law in the reference frame R_B, as (3):

$$\begin{cases} m\left(\frac{d\vec{V}_{B/R_0}}{dt}\right)_{/R_B} = \vec{F}_{/R_B} - m(\vec{\Omega}_{R_B/R_0} \wedge \vec{V}_{B/R_0}) \\ \Pi_{B/G} \cdot \dot{\vec{\Omega}}_{R_B/R_0} = \vec{M}_G - \vec{\Omega}_{R_B/R_0} \wedge \Pi_{B/G} \cdot \vec{\Omega}_{R_B/R_0} \end{cases} \qquad (3)$$

with:
- m: mass of the sailboat
- $\Pi_{B/G}$: inertial matrix of the sailboat
- $\vec{V}_{B/R_0}$: velocity vector of CoG in R_0
- $\vec{\Omega}_{R_B/R_0}$: angular velocity vector in R_0
- $\vec{M}_G$: total torque acting on the sailboat.

R_0 is an Earth-fixed inertial frame and R_B is a Body-fixed reference frame, with its origin at the ship's center of gravity (CoG).

From this analytical description of the dynamics of our sailboat, a numerical simulator has been built, which integrates the differential equations of motion using a classical Runge-Kunta algorithm. This numerical simulator can then be used to simulate the behaviour of our prototype under different environmental conditions (see section IV).

The numerical model can also be used to compute the speed polar diagram of the sailboat (see Fig. 2). These performance curves correspond to the steady-state velocity of the vehicle for a given wind speed and a given wind direction and for headings varying from 45° to 315°. To keep a constant heading with respect to the wind until the simulation reaches the steady-state for the vehicle velocity, a PID controller on the rudder and on the boom has been used.

For wind speeds varying from 5 to 20 Knots, speed profiles look similar. A so-called *upwind no-go zone* is discarded for $-45° \leq \varphi \leq 45°$. Another "touchy" sailing zone, called *downwind no-go zone*, is exhibited for $150° \leq \varphi \leq 210°$. In fact the boat is able to navigate in this region, but for safety reasons (instability) these headings will also be avoided in practice. The performance curves will also be used to trim the sail angle in real-time to reach a given reference in terms of vehicle velocity and heading for given wind speed and direction. The description of this sail trimming algorithm is out of the scope of this article.

A high potential will be affected to these upwind and downwind sailing regions in the path planner presented in next section.

2011, 15th Int. Conf. on Advanced Robotics (ICAR'11), Pages 112-117, Tallinn, Estonia 2011.
DOI : 10.1109/ICAR.2011.6088585

III. PATH PLANNING

In the recent years, numerous method have been proposed for the path planning of autonomous sailboat robots : based on logic rules [18], [19], state machine [20]–[22], neural control [23] or ray-tracing techniques for path planning with obstacles avoidance [24].
On the other hand, potential fields methods, due to Khatib [25] and Krogh [26], have been successfully employed for robot control and motion planning of mobile robots (see for example [27]–[30] among many others).

In artificial potential fields methods, movements of the robot (represented as a particle) are governed by a field which is usually composed of two components, an attractive potential drawing the robot towards the goal and a repulsive potential pushing the robot away from obstacles. The originality of our method is to build a so-called local potential around the boat location to take upwind and downwind constraints into account. An hysteresis potential relative to the cost of tackling and jibing is also proposed, which makes our method easy to tune according to the vehicle specifications.

The main drawback with this technique is its susceptibility to local minima. However, typical marine environments are sparse and local minima in this case are not an issue. The reliability of our path planning method will rather benefit from coupling this high-level path planning technique with a low-level realistic simulator derived from the sailboat model identified in section II.

A. Potential field approach

Our potential field approach is decomposed in two parts, a global potential field and a local potential field. The global potential field is relative to the goal point and the obstacles. The local potential field is relative to the wind direction (true wind angle, TWA).

1) Global potential: The global potential is built on the all map once for all at the beginning of the planing process. It aims at attracting the vehicle towards the goal point and repulsing the vehicle outwards the obstacles.

a) Potential relative to the goal point: In order to attract the vehicle towards the goal point a linear potential P_g is built for every point P of the map as follows:

$$P_g = G_g.dist(P,P_g)$$

where G_g is the desired gradient and $dist(P,P_g)$ is the Euclidean distance between P and the goal point P_g. Since G_g is a constant, the potential P_g looks like a cone centered on P_g (see Fig. 3).

b) Potential relative to the obstacles: A repulsive potential relative to the obstacles P_o is built for every point P of the map as follows:

$$P_o = \frac{k}{dist(P,P_o)}$$

where k is a tunable scalar. This potential tends to infinite as we come close to the obstacles, which prevents the vehicle to go through the obstacles.

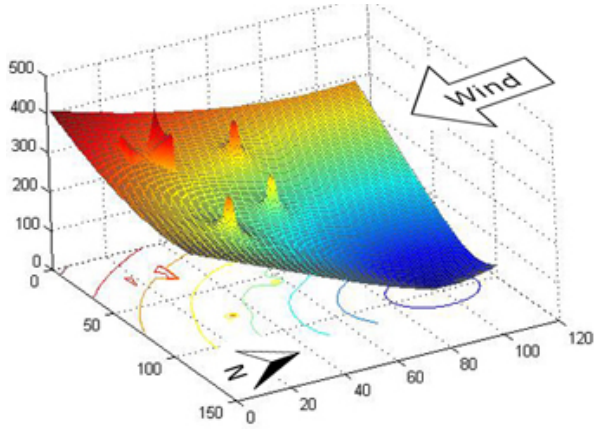

Fig. 3. Illustration of the global potential relative to the goal point and relative to the obstacles. In this case the upwind no-go zone is pointing up because the wind is coming from North.

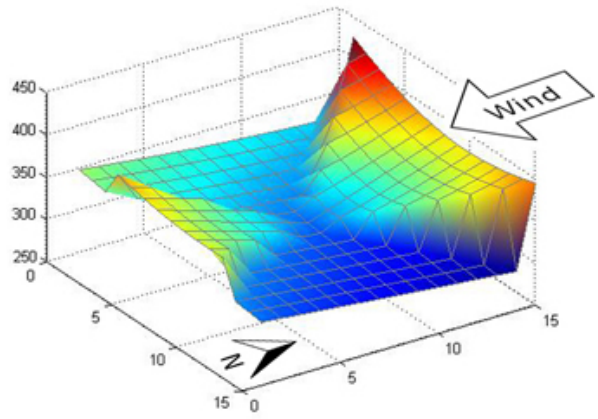

Fig. 4. Close-up on the local potential around the boat.

2) Local potential: The local potential is built in the neighborhood of the boat location. It is rebuilt after each displacement of the boat according to the wind direction and the latest tack.

a) Upwind potential: In order to take the upwind no-go zone into account a so-called upwind potential P_{up} is built dynamically for each point P_w inside a window centered on the boat location P. The magnitude of P_{up} is a function of the angle ϕ between the direction of $P\vec{P}_w$ and the wind direction TWA. It is linear inside the upwind no-go zone sector (defined by the angle ϕ_{up}, see Fig. 5) and null outside:

$$\begin{cases} P_{up} = G_{up}.dist(P_w,P) & \text{if } 0 < |\phi| < \phi_{up} \\ P_{up} = 0 & \text{elsewhere} \end{cases}$$

b) Downwind potential: In order to take the downwind no-go zone into account a so-called downwind potential P_{down} is built dynamically for each point P_w inside the same window centered on the boat location P. The magnitude of P_{down} is a function of the angle between the boat direction ϕ and the wind direction TWA. It is linear inside the downwind no-go zone sector (defined by the angle ϕ_{down}, see Fig. 5)

2011, 15th Int. Conf. on Advanced Robotics (ICAR'11), Pages 112-117, Tallinn, Estonia 2011.
DOI : 10.1109/ICAR.2011.6088585

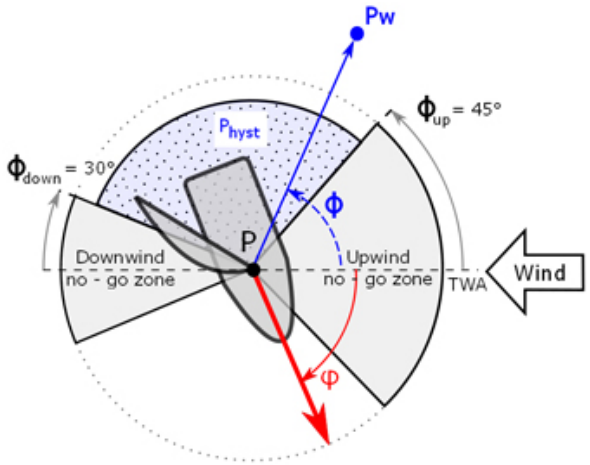

Fig. 5. Scheme of the upwind and downwind no-go zones. The dotted region corresponds to the region where $P_{hyst} \neq 0$

and null outside:

$$\begin{cases} P_{down} = G_{down}.dist(P_w,P) & \text{if } 0 < |\phi - \pi| < \phi_{down} \\ P_{down} = 0 & \text{elsewhere} \end{cases}$$

c) Jibe and tackle potential: In order to take the cost of jibing and tackling into account a so-called hysteresis potential P_{hyst} is built dynamically for each point P_w inside the window centered on the boat location P. The magnitude of P_{hyst} is a function of the angle ϕ and the latest tack. If the boat navigates with the wind coming from the left, P_{hyst} will be defined at the right side of the wind direction (see Fig. 5) to prevent the boat to tack or jibe too frequently. In the case of wind coming from the left, P_{hyst} is defined as follows:

$$\begin{cases} P_{hyst} = G_{hyst}.dist(P_w,P) & \text{if } \phi_{up} < \phi < \pi - \phi_{down} \\ P_{hyst} = 0 & \text{elsewhere} \end{cases}$$

where the gradient G_{hyst} of the potential P_{hyst} is tunable.

3) Potential descent: Once the local potential has been built and added to the global potential, a potential descent is carried out to find the new heading for the boat. Practically, a profile of the potential around the boat location P is extracted along a ring centered in P with a radius R defined as a function of the window size W_{size}: $R = W_{size} - 1$. The heading φ for the next move is the angle corresponding to the global minimum of the profile. The potential descent algorithm is stopped when the boat arrives in the vicinity of the goal point. Precisely, the stop criteria is defined as follows: $dist(P_g,P) < \varepsilon$, with $\varepsilon = W_{size} + 1$.

B. Simulation results

In this section, the influence of wind configurations and sailboat capabilities on trajectories will be analyzed in simulation. Realism of resulting trajectories from our reactive path planning approach will eventually be discussed.

1) Simulated environment: For the sake of clarity, the environment in the following simulations is assumed to be static (obstacles are fixed) and completely known (obstacles are mapped without uncertainty). Besides, the wind is assumed to be constant in direction as well as in velocity. However, since our local potential is incrementally built as a function of the visible wind and obstacles around the boat location, this reactive path planning approach holds for dynamic environments and can be implemented without any change on real embedded systems.

In this section, default parameters for the potential are set up as follows: $G_{goal} = 3$, $G_{up} = 10$, $G_{down} = 5$, $G_{hyst} = 2$, $k = 100$, $\theta_{up} = 45°$, $\theta_{down} = 30°$.

2) Simulated trajectories:

a) Downwind navigation: Fig. 6 depicts the trajectory solutions exhibited by the potential field based path planner for winds coming from West and from South-West.

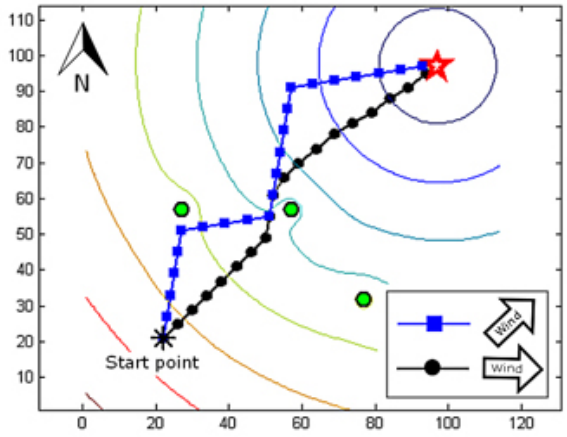

Fig. 6. Trajectory computed with winds coming from West and South-West

In case of wind coming from West, the sailboat navigates directly towards the goal point while avoiding obstacles without any difficulty. In case of wind coming from South-West, the optimal trajectory in respect with the potentials built by our planner is more complex. The boat avoids two obstacles and executes three jibes on its way to the goal point.

b) Upwind navigation: Fig. 7 depicts the trajectory solution exhibited by the potential field based path planner for a wind coming from North-East. Several hysteresis potentials have been tested. The red trajectory has been computed with $G_{hyst} = 3$, the blue trajectory has been computed with $G_{hyst} = 2$ and the black trajectory has been computed with $G_{hyst} = 1$. Two, three and seven tackles have been respectively executed to reach the goal point.

c) Conclusion: The presented path planner provides coherent trajectories in terms of heading constraints for a sailboat. Trajectories follow admissible headings regarding the upwind and downwind no-go zones. The number of jibes and tackles may be tuned by the hysteresis potential to suit the real cost of these manoeuvres. Besides, attractiveness of the goal point and repulsiveness of obstacles are easily tunable in this potential field framework.

2011, 15th Int. Conf. on Advanced Robotics (ICAR'11), Pages 112-117, Tallinn, Estonia 2011.
DOI : 10.1109/ICAR.2011.6088585

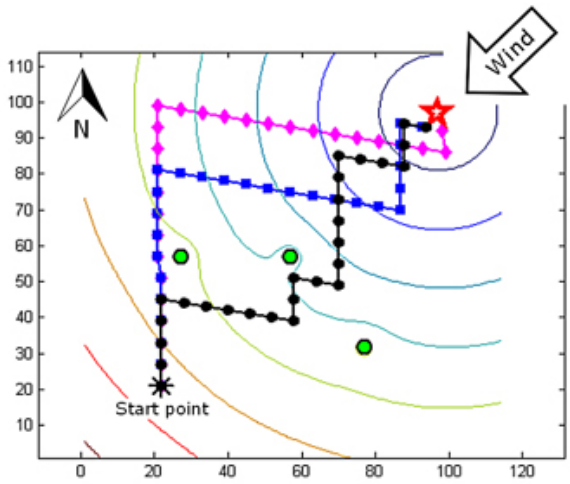

Fig. 7. Trajectories computed with the wind coming from North-East using different hysteresis potentials. In red $G_{hyst} = 3$, in blue $G_{hyst} = 2$, in black $G_{hyst} = 1$

IV. Numerical path planning validation

In this section, realism of the simulations will be improved in terms of external environment and internal model of the boat. For this purpose, a spatially variable wind field will be introduced and the dynamic model of the sailboat identified in section II will be used.

A. Realistic environment

In this section the path planner is tested using a more realistic model of a marine wind field. As depicted in Fig. 8) the wind in this path planning simulation varies from West to East along the x-axis. The trajectory exhibited by the potential field based path planning algorithm bends to the East as the wind turns from West to North up to a point where a tackle becomes necessary to reach the goal point.

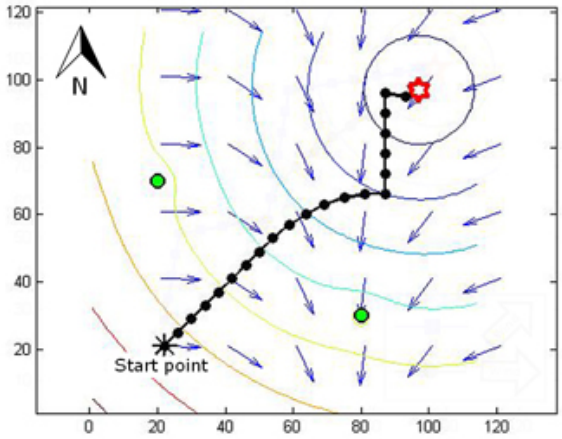

Fig. 8. An example of trajectory computed with a dynamic wind field

B. Realistic boat model

In the simulations so far the vehicle dynamics has been neglected. Resulting paths extracted from the start to the goal point point may not be physically admissible for a given sail boat. Even if these trajectories can be considered from a high level point of view, introducing the sailboat dynamics would greatly improve the reliability of the overall path planning method. For this reason a numerical simulator will be coupled with our path planner to give us more realistic simulations.

1) Simulator description: The numerical simulator developed in section II is called as a DLL library. Inputs at step n are the attitude (roll, pith and yaw), position (x, y, z), linear and angular speeds of the boat, the boom angle, the rudder angle, true wind angle and true wind speed. Outputs are the same variables at step $n+1$. In the following simulations the state of the boat is initialized at zero for the linear and angular speed as well as for the attitude and the boat is pointing towards the goal point. The low-level control loop for the boom angle and for the rudder angle is a simple PID controller that makes the heading converging to the heading reference given by the high-level path planner.

2) Results: A comparison between trajectory computed using only the high-level path planner and a trajectory resulting from the coupling of the path planner with the low-level simulator is given in Fig. 9. In this framework, where the wind comes from East, the boat begins to accelerate in the direction given by the path planner. At this stage of the simulation both trajectories are similar in terms of heading. To reach the target a jibe is theoretically necessary at some point of the trajectory (see the black curve). While easily done when neglecting the vehicle dynamics, this manoeuver is far from immediate in practice. The inertia of the boat may impact such a turn in the trajectory, as depicted by the blue curve.

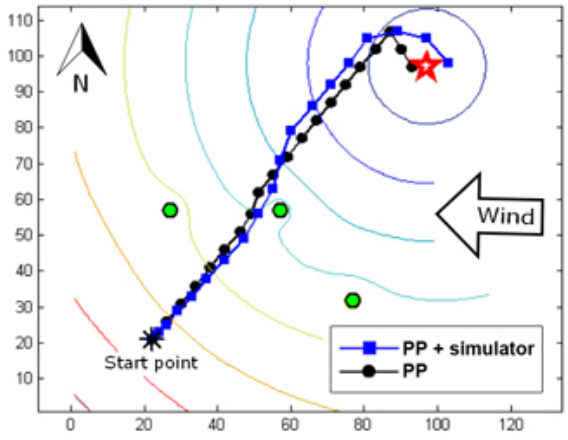

Fig. 9. Trajectories computed with the high level path planner only (PP) and by coupling the high level path planner and the low level simulator (PP + simulator)

2011, 15th Int. Conf. on Advanced Robotics (ICAR'11), Pages 112-117, Tallinn, Estonia 2011.
DOI : 10.1109/ICAR.2011.6088585

V. Conclusion and future works

In this work, we have presented a reactive path planning method for the navigation of a sailboat autonomous robot. This path planning algorithm, based on potential field method, reacts to changing wind conditions as well as detected obstacles in real-time by recalculating the heading periodically. This method have been successfully tested and validated in simulation under various wind conditions, using a computational efficient numerical simulator specifically tuned for the boat that we will use in the next future.
This 3.6 m long sailboat based on a mini-J hull (a reduced scale of a 12M JI class) is currently under development (see Fig. 10). The electrical power is provided by a battery pack, charged by a windmill and a 0.5 m^2 solar panel. She will use on-board navigation sensors (IMU, GPS, anemometer and wind vane) as well as perception sensors (sonar, hydrophones and panoramic camera) for obstacles detection.

Fig. 10. First field test trial of the sailboat

References

[1] J. Manley, "Unmanned surface vehicles, 15 years of development," in *MTS/IEEE OCEANS 2008*, 2008.
[2] M. Robin, S. Eric, G. Chandler, C. Charlie, H. Mike, and P. Kevin, "Cooperative use of unmanned sea surface and micro aerial vehicles at hurricane wilma," *Journal of Field Robotics*, vol. 25, no. 3, pp. 164–180, 2008.
[3] T. Pastore and V. Djapic, "Improving autonomy and control of autonomous surface vehicles in port protection and mine countermeasure scenarios," *Journal of Field Robotics*, vol. 27, no. 6, pp. 903–914, 2010.
[4] P. Mahacek, T. Berk, A. Casanova, C. Kitts, W. Kirkwood, and G. Wheat, "Development and initial testing of a swath boat for shallow-water bathymetry," in *MTS/IEEE OCEANS 2008*, 2008.
[5] E. Steimle and M. Hall, "Unmanned surface vehicles as environmental monitoring and assessment tools," in *MTS/IEEE OCEANS 2006*, 2006.
[6] P. Mahacek, R. Kobashigawa, A. Schooley, and C. Kitts, "The wasp: an autonomous surface vessel for the university of alaska," in *MTS/IEEE OCEANS 2005*, 2005, pp. 2282 – 2291 Vol. 3.
[7] M. Caccia, R. Bono, G. Bruzzone, E. Spirandelli, G. Veruggio, A. Stortini, and G. Capodaglio, "Sampling sea surfaces with sesamo: an autonomous craft for the study of sea-air interactions," *IEEE Robotics Automation Magazine*, vol. 12, no. 3, pp. 95 – 105, 2005.
[8] A. Pascoal, P. Oliveira, C. Silvestre, and et al, "Robotic ocean vehicles for marine science applications: the european asimov project," in *MTS/IEEE OCEANS 2000*, 2000, pp. 409–415 vol.1.
[9] A. Dhariwal and G. Sukhatme, "Experiments in robotic boat localization," in *IEEE/RSJ Int. Conf. on Intelligent Robots and Systems*, 2007, pp. 1702 –1708.
[10] G. Podnar, J. Dolan, A. Elfes, S. Stancliff, E. Lin, J. Hosier, T. Ames, J. Moisan, T. Moisan, J. Higinbotham, and E. Kulczycki, "Operation of robotic science boats using the telesupervised adaptive ocean sensor fleet system," in *IEEE Int. Conf. on Robotics and Automation*, 2008, pp. 1061 –1068.
[11] J. Curcio, J. Leonard, and A. Patrikalakis, "Scout - a low cost autonomous surface platform for research in cooperative autonomy," in *MTS/IEEE OCEANS 2005*, 2005, pp. 725 – 729 Vol. 1.
[12] D. Eickstedt, M. Benjamin, H. Schmidt, and J. Leonard, "Adaptive control of heterogeneous marine sensor platforms in an autonomous sensor network," in *IEEE/RSJ Int. Conf. on Intelligent Robots and Systems*, 2006, pp. 5514 –5521.
[13] N. Cruz and J. Alves, "Autonomous sailboats: An emerging technology for ocean sampling and surveillance," in *MTS/IEEE OCEANS 2008*, 2008.
[14] P. Rynne and K. von Ellenrieder, "A wind and solar-powered autonomous surface vehicle for sea surface measurements," in *OCEANS 2008*, 2008.
[15] D. Harris, G. Thomas, and M. Renilson, "Downwind performance of yachts in waves," in *2nd Australian Sailing Science Conference*, 1999.
[16] J. Gerritsma, J. Keuning, and R. Onnink, "Results and analysis of the delft systematic series ii yacht hull form experiments," in *11th HISWA Int. Symp. on Yacht Design and Yacht Construction*, 1990.
[17] E. Jacquin, Y. Roux, P.-E. Guillerm, and B. Alessandrini, "Toward numerical vpp with the full coupling of hydrodynamic and aerodynamic solvers for acc yacht," in *17 Chesapeake Sailing Yatch Symposium*, 2005.
[18] M. Neal, "A hardware proof of concept of a sailing robot for ocean observation," *IEEE Journal of Oceanic Engineering*, vol. 31, no. 2, 2006.
[19] R. Stelzer and T. Proll, "Autonomous sailboat navigation for short course racing," *Robotics and Autonomous Systems*, vol. 56, no. 7, pp. 604 – 614, 2008.
[20] Y. Briere, F. L. Cardoso Ribeiro, and M. Vieira Rosa, "Design methodologies for the control of an unmanned sailing robot," in *8th Conf. on Manoeuvring and Control of Marine Craft*, 2009.
[21] G. Elkaim and C. Boyce, "Energy scavenging and aerodynamic performance of a rigid wing propulsion system for an autonomous surface vessel," in *ION Global Navigation Satellite Systems Conference*, 2009.
[22] H. Erckens, G.-A. Busser, C. Pradalier, and R. Siegwart, "Avalon: Navigation strategy and trajectory following controller for an autonomous sailing vessel," *IEEE Robotics Automation Magazine*, vol. 17, no. 1, pp. 45 –54, 2010.
[23] C. Sauze and M. Neal, "A neuro-endocrine inspired approach to long term energy autonomy in sailing robots," in *Proc. TAROS 2010 : Towards Autonomous Robotic Systems*, 2010.
[24] R. Stelzer, K. Jafarmadar, H. Hassler, and R. Charwot, "A reactive approach to obstacle avoidance in autonomous sailing," in *3rd Int. Robotic Sailing Conference*, 2010.
[25] O. Khatib, "Real-time obstacle avoidance for manipulators and mobile robots," *International Journal of Robotics Research*, vol. 5, no. 1, pp. 90–98, 1986.
[26] B. Krogh and C. Thorpe, "Integrated path planning and dynamic steering control for autonomous vehicles," in *IEEE Int. Conf. on Robotics and Automation*, vol. 3, 1986, pp. 1664–1669.
[27] J. Barraquand, B. Langlois, and J.-C. Latombe, "Numerical potential field techniques for robot path planning," *IEEE Transactions on Systems, Man and Cybernetics*, vol. 22, no. 2, pp. 224 –241, 1992.
[28] H. Haddad, M. Khatib, S. Lacroix, and R. Chatila, "Reactive navigation in outdoor environments using potential fields," in *IEEE Int. Conf. on Robotics and Automation*, vol. 2, 1998, pp. 1232 –1237.
[29] S. Ge and Y. Cui, "Dynamic motion planning for mobile robots using potential field method," *Autonomous Robots*, vol. 13, no. 3, pp. 207 –222, 2002.
[30] S. Shimoda, Y. Kuroda, and K. Iagnemma, "Potential field navigation of high speed unmanned ground vehicles on uneven terrain," in *IEEE Int. Conf. on Robotics and Automation*, 2005, pp. 2828 – 2833.